Generation of Ultrasound Pulses in Water using Granular Chains with a Finite Matching Layer

Sevan Harput,[1] James McLaughlan,[1,2] David M. J. Cowell,[1] Pierre Gelat,[3] Nader Saffari,[3] Jia Yang,[4] Omololu Akanji,[4] Peter J. Thomas,[4] David A. Hutchins,[4] and Steven Freear[1]

[1)] *Ultrasonics and Instrumentation Group, School of Electronic and Electrical Engineering, University of Leeds, Leeds, LS2 9JT, UK.*

[2)] *Division of Biomedical Imaging, University of Leeds, Leeds, LS2 9JT, UK.*

[3)] *Department of Mechanical Engineering, University College London, Torrington Place, London WC1E 7JE, UK.*

[4)] *School of Engineering, University of Warwick, Coventry CV4 7AL, UK.*

Wave propagation in granular chains is subject to dispersive effects as well as to nonlinear effects arising from the Hertzian contact law. This enables the formation of wideband pulses, which is a desirable feature in the context of diagnostic and therapeutic ultrasound applications. However, coupling of the ultrasonic energy from a chain of spheres into biological tissue is a big challenge. In order to improve the energy transfer efficiency into biological materials, a matching layer is required. A prototype device was designed to address this by using six aluminium spheres and a vitreous carbon matching layer. The matching layer and the pre-compression force are selected specifically to maximise the acoustic pressure in water and its bandwidth. The designed device generated a train of wideband ultrasonic pulses from a narrowband input with a centre frequency of 73 kHz.

An analytical model was created to simulate the behaviour of a matching layer as a flexible thin plate clamped from the edges. This model was then verified using free field hydrophone measurements in water, which successfully predicted the increased bandwidth by generation of harmonics. The shapes of the measured and the predicted waveforms were compared by calculating the normalised cross-correlation, which showed 83% similarity between both. Since the generation of harmonics are of interest for this study, the total harmonic distortion (THD) and the -6 dB bandwidth of the signals were used to analyse signal fidelity between the hydrophone measurements and the model predictions. The acoustic signals in water had a root mean squared THD of 73% and the model predicted a root mean squared THD of 78%. The -6 dB bandwidths of individual pulses measured by a hydrophone and predicted with the model were 280 kHz and 252 kHz, respectively. At these high ultrasonic frequencies, it is the first experimental demonstration of resonant chains operating in water with a matching layer.

I. INTRODUCTION

Wave propagation in homogeneous granular chains and interactions of spherical elastic objects have been well studied both theoretically and experimentally[1–5]. In such a system with Hertzian contact, a nonlinear force-deformation relation exists as $F \propto \delta^{1.5}$. This nonlinear behaviour can reshape the input of the system and generate wideband impulses similar to acoustic metamaterials and super-lenses, which attract great attention due to their potential for improving spatial resolution beyond the diffraction limit[6]. It is also possible to use this nonlinear behaviour in granular chains for acoustic switching and rectification via spectral bifurcation of certain frequencies into new broadband frequency components[7].

Multiple spherical chains can be used to form a nonlinear acoustic lens in a variety of applications such as biomedical imaging, non-destructive evaluation, underwater mapping, and shock absorbers[8–10]. Generation of wideband short duration pulses is desirable both in diagnostic and therapeutic ultrasound. Wideband pulses improve the diagnostic image resolution and the functionality of other ultrasound modalities, such as harmonic imaging and multiple excitation techniques[11–14]. In ultrasound therapy, short duration monopolar ultrasonic pulses can create a spatially-concentrated high energy region, which will minimise the potential collateral damage in the surrounding healthy tissue[15].

Granular chains possess waveguide-like effects, such as turning corners and robust propagation under deflection[16]. The propagation characteristics, such as the propagation speed, can be tuned by changing the pre-compression force in the chain, the particle material or size. By using multiple granular chains, it is possible to focus and steer ultrasound waves[8,9,17], which makes granular chains suitable for biomedical ultrasound applications by increasing the output pressure and the frequency. This study is therefore focusing on maximising the transferred energy from a chain of spheres into biological tissue and also the harmonic content, which increases the bandwidth of the generated ultrasound waves.

After Nesterenko's pioneering work in 1983, a great number of models were developed to simulate wave propagation in infinite and finite chains[1,2,4,18]. However, predicting the resonance behaviour in harmonically driven monoatomic granular chains, modelling the nonlinear and dispersive effects, and minimizing the overall structure are still big challenges [5,19]. In addition to this, the problem becomes more complicated once the chain is coupled into a finite material, where a matching layer is essential for biomedical applications. It is known that

$$m\ddot{x}_1 = \frac{4\sqrt{R}}{3}\theta_{t\text{-}s}\left(\delta_{t\text{-}s}+x_t-x_1\right)^{\frac{3}{2}} - \frac{\sqrt{2R}}{3}\theta_s\left(\delta_{s\text{-}s}+x_1-x_2\right)^{\frac{3}{2}} + \lambda(\dot{x}_t-\dot{x}_1)\,H(\delta_{t\text{-}s}+x_t-x_1) - \lambda(\dot{x}_1-\dot{x}_2)\,H(\delta_{s\text{-}s}+x_1-x_2) \quad (1)$$

$$m\ddot{x}_i = \frac{\sqrt{2R}}{3}\theta_s\left(\delta_{s\text{-}s}+x_{i-1}-x_i\right)^{\frac{3}{2}} - \frac{\sqrt{2R}}{3}\theta_s\left(\delta_{s\text{-}s}+x_i-x_{i+1}\right)^{\frac{3}{2}} + \lambda(\dot{x}_{i-1}-\dot{x}_i)\,H(\delta_{s\text{-}s}+x_{i-1}-x_i) - \lambda(\dot{x}_i-\dot{x}_{i+1})\,H(\delta_{s\text{-}s}+x_i-x_{i+1}) \quad (2)$$

$$m\ddot{x}_n = \frac{\sqrt{2R}}{3}\theta_s\left(\delta_{s\text{-}s}+x_{n-1}-x_n\right)^{\frac{3}{2}} - \frac{4\sqrt{R}}{3}\theta_{m\text{-}s}\left(\delta_{m\text{-}s}+x_n-x_m\right)^{\frac{3}{2}} + \lambda(\dot{x}_{n-1}-\dot{x}_n)\,H(\delta_{s\text{-}s}+x_{n-1}-x_n) - \lambda_{\text{rest}}(\dot{x}_n-\dot{x}_m)\,H(\delta_{m\text{-}s}+x_n-x_m) \quad (3)$$

$$\frac{m_m}{4}\ddot{x}_m = \frac{4\sqrt{R}}{3}\theta_{m\text{-}s}(\delta_{m\text{-}s}+x_n-x_m)^{\frac{3}{2}} + (\lambda_m+\lambda_{\text{rest}})\,(\dot{x}_n-\dot{x}_m)\,H(\delta_{m\text{-}s}+x_n-x_m) - K_m x_m - \lambda_m\dot{x}_m \quad (4)$$

the wave interaction with boundaries depend on wall mechanical properties[20]. Coupling into a thin matching layer further increases the complexity of the existing problem, since the properties of the reflected and transmitted waves are significantly affected by both the material and its thickness[10].

A prototype device was developed based on this nonlinearity in a one-dimensional chain of spheres by Hutchins *et al.*[18,21–23]. The developed transducer is able to transform a narrowband sinusoidal input force into a train of wideband impulses at ultrasonic frequencies. Donahue *et al.* and Harput *et al.* presented generation of ultrasound waves in water by using a granular chain with a matching layer[17,24,25]. However, neither of these studies analysed the energy transfer from a chain of spheres into biological tissue in detail.

In this study, a matching layer was modelled as a flexible thin circular disc clamped from the edges and merged into an existing analytical model[18,26] to identify suitable materials for biomedical applications. Different matching materials, such as glass, aluminium, acrylic, silicon rubber, and vitreous carbon, were analysed with this model. The chosen matching material was attached to the aforementioned prototype device. Results achieved with this model were verified against hydrophone measurements.

II. MATERIALS AND METHODS

A. New Model with a Matching Layer

An analytical model created by Hutchins *et al.*[18], and later analysed in greater depth by Yang *et al.*[26], was used to simulate the wave propagation through the chain. The existing model, that places an infinite wall behind the last sphere, was modified to implement the effect of the matching layer at the end of the chain. The matching layer was modelled as a flexible thin plate clamped from the edges incorporated into the model as given in (4). Equations (1), (2), and (3) describe the motion of the first sphere, middle spheres, and the last sphere for a granular chain consist of n-spheres with variables explained in Table I.

The effective Young's modulus of the spheres, ultrasonic horn and matching layer are defined as

$$\theta_t = \frac{E_t}{1-{\nu_t}^2}, \quad \theta_s = \frac{E_s}{1-{\nu_s}^2}, \quad \theta_m = \frac{E_m}{1-{\nu_m}^2}\,. \quad (5)$$

The effective Young's modulus associated with contact

TABLE I. Nomenclature

Symbol	Parameter Definition	Unit
x	displacement of *	m
$\dot{x}$	velocity of *	m/s
$\ddot{x}$	acceleration of *	m/s^2
$\dot{x}_f$	output velocity at the surface	m/s
m	mass of a single sphere	kg
m_m	mass of the matching layer	kg
R	radius of the sphere	m
R_m	radius of the matching layer	m
h_m	thickness of the matching layer	m
K_m	spring coefficient of the matching layer	N/m
λ	damping of spheres	N·s/m
λ_m	damping of the matching layer	N·s/m
λ_{rest}	damping due to restitutional motion	N·s/m
F_0	pre-compression force	N
ρ	density of *	kg/m^3
E	Young's modulus of *	Pa
ν	Poisson's ratio of *	
θ	effective Young's modulus of *	Pa
δ	overlap between different materials *	m
Z	acoustic impedance of *	MRayl
$H()$	Heaviside function	

* subscripts represent the following: 1 is the first sphere, i is the i-th sphere, n is the last sphere, s is any sphere, t is the ultrasonic horn, and m is the matching layer.

interactions between the first sphere and the ultrasonic horn is represented with $\theta_{t\text{-}s}$ and the same parameter between the last sphere and the matching layer is represented with $\theta_{m\text{-}s}$, which are defined as

$$\frac{1}{\theta_{t\text{-}s}} = \frac{1}{\theta_t} + \frac{1}{\theta_s}, \qquad \frac{1}{\theta_{m\text{-}s}} = \frac{1}{\theta_m} + \frac{1}{\theta_s}\,. \tag{6}$$

The pre-compression force creates small elastic deformations, which result in an overlap of the hypothetical boundaries between the components of the system without any deformations. The overlap between spheres is denoted as $\delta_{s\text{-}s}$, overlap between the first sphere and the ultrasonic horn is denoted as $\delta_{t\text{-}s}$, and overlap between the last sphere and the matching layer is denoted as $\delta_{m\text{-}s}$. These parameters depend on the pre-compression force applied to the chain as

$$\delta_{t\text{-}s}=\left(\frac{3F_0}{4\sqrt{R}\theta_{t\text{-}s}}\right)^{\frac{2}{3}},\ \delta_{s\text{-}s}=\left(\frac{3F_0}{\sqrt{2R}\theta_s}\right)^{\frac{2}{3}},\ \delta_{m\text{-}s}=\left(\frac{3F_0}{4\sqrt{R}\theta_{m\text{-}s}}\right)^{\frac{2}{3}}. \tag{7}$$

For the equation of motion of the matching layer given in (4), the first line of the equation describes the forces involved when the last sphere and the matching material are in contact, such as the Hertzian contact force and the deflection of the matching layer. The second line of the equation describes the free vibrations of the matching material as a thin plate clamped from the edges with an effective mass of $m_m/4$, when the last sphere and matching layer are not in contact.

Deflection of a thin circular plate with clamped edges under a central load F_0 can be calculated according to the spring coefficient K_m as

$$\xi_m = \frac{F_0}{K_m}, \text{ where } K_m = \frac{4\pi\theta_m h_m^3}{3R_m^2}\,. \tag{8}$$

Vibrations of the matching plate were damped by λ_m when not in contact with the last sphere, and damped by $\lambda_m + \lambda_{\text{rest}}$ when in contact with the last sphere. Yang *et al.*[10] suggested to use the inelasticity parameter λ_{rest} to calculate the restitutional motion of the striker on a plate, which is determined by the material properties and geometry of the last sphere and the matching layer as

$$\lambda_{\text{rest}} = \frac{\pi^{0.6}}{4\sqrt{3}}\left(\frac{2R}{h_m}\right)^2\left(\frac{\rho_s}{\rho_m}\right)^{0.6}\left(\dot{x}_n\sqrt{\frac{\rho_m}{\theta_m}}\right)^{0.2}\left(\frac{\theta s}{\theta s+\theta m}\right)^{0.4} \tag{9}$$

After deriving the equation of motions for the spheres and the matching layer, the mechanism of wave coupling into water was modelled as a superposition of waves propagating through the matching layer and vibrations of the matching layer as a thin plate. The propagated wave through the aluminium sphere into matching layer and then from matching layer to water was attenuated due to impedance mismatch between these layers as;

$$T_m = 1-\left(\frac{Z_m - Z_s}{Z_m + Z_s}\right)^2,\ T_w = 1-\left(\frac{Z_w - Z_m}{Z_w + Z_m}\right)^2 \tag{10}$$

The final velocity at the surface of the matching layer, $\dot{x}_f$, was calculated as the superposition of the last sphere's and matching layer's velocities as

$$\dot{x}_f = \dot{x}_n\sqrt{T_m T_w}H(\delta_{m\text{-}s} + x_n - x_m) + \dot{x}_m \tag{11}$$

The first term in Eq. (11) is the velocity of the last sphere coupled to the matching layer and then water, while the last sphere is in contact with the matching layer. The transmitted energy is scaled by T_m into the matching layer, and T_w into the water. The second term represents the velocity of the matching layer.

To reduce the complexity of the model the following assumptions were made. The matching layer was modelled as a flexible thin circular disc clamped from the edges with an effective mass of $m_m/4$. The Doppler effects due to the vibrations of the matching layer were ignored due to the large difference between the Doppler frequency and the output frequency of the system. The effect of nonlinear propagation of ultrasound waves in water was not incorporated into the model, since both the amplitude of the pressure wave and the ultrasonic frequency were low. The attenuation inside the matching material was ignored. Parameters used in the analytical model for different matching materials, spheres, and ultrasonic horn were assumed to be the generic material properties given in Table II.

B. Experimental Setup

The experimental setup with the granular chain system and a membrane hydrophone is illustrated in Figure 1. A granular chain containing 6 aluminium spheres with a diameter of 1 mm was placed into a holder. The holder was manufactured from an R11 polymer by using the Digital Light Processing (DLP) technique with an EnvisionTEC Perfactory Mini Multi Lens 3D Printer (Envisiontec Inc., Dearborn, MI) to enhance the solitary wave behaviour as explained by Akanji *et al.*[23]. The chain of spheres and the ultrasonic horn was fixed on two separate assemblies, where a high precision micro-meter translation stage with a differential adjuster (Thorlabs, Newton, NJ) was used to adjust the static pre-compression

TABLE II. Material parameters used in the analytical model

	Density (kg/m^3)	Young's Modulus (GPa)	Poisson's Ratio	Acoustic Impedance (MRayl)
Aluminium	2700	69	0.33	17.3
Stainless steel	7800	200	0.30	45.7
Vitreous carbon	1540	35	0.15	7.4
Acrylic	1200	2.5	0.35	3.2
RTV silicone	1100	0.1	0.49	1.4
Water	1000			1.5

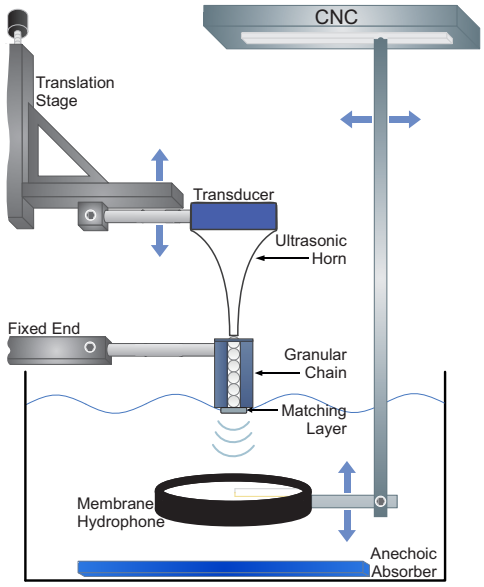

FIG. 1. Illustration of the experimental setup. Transducer, ultrasonic horn, granular chain assembly and the matching layer together form a nonlinear system that can generate wideband impulses. A membrane hydrophone is used to measure acoustic pressure waveform generated by this system. A CNC is used to control the alignment of the hydrophone. The pre-compression force is adjusted with a high precision micrometer translation stage. The granular chain is exaggerated for easier visualisation.

force. The input into the granular chain was generated by an ultrasonic transducer attached to a stainless steel ultrasonic horn to amplify the pressure waves generated by this transducer. A matching layer was placed on the other side of the chain to increase the coupling efficiency into water. A 0.5 mm thick vitreous carbon disc with a diameter of 12 mm was chosen as a matching layer with the given parameters in Table II. The system was partially submersed in degassed and deionized water for pressure measurements. The acoustic pressure generated by the granular chain was measured in water using a Polyvinylidene Fluoride (PVDF) differential membrane hydrophone (Precision Acoustics Ltd., Dorchester, UK) controlled by a CNC.

The transducer and the stainless steel ultrasonic horn with a fundamental frequency of 73 kHz was used to generate narrowband signals as an input into the chain of spheres. A 25 cycle sinusoidal tone burst with a central frequency of 73 kHz was generated by a 33600A True-Form Waveform Generator (Agilent Technologies Inc., Santa Clara, CA). This input waveform was amplified to 600 Vpp by a 2200L Power Amplifier (Electronics & Innovation Ltd., Rochester, NY) before exciting the transducer. The displacement and the velocity profile at the tip of the ultrasonic horn was measured by a PSV-500 Scanning Vibrometer (Polytec GmbH Waldbronn, Germany). The measured displacement and velocity profiles by the Laser vibrometer were used as an input into the

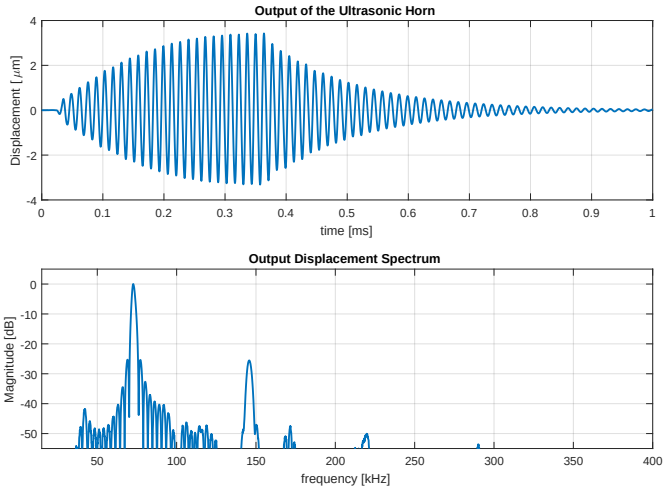

FIG. 2. (Top) Displacement profile measured at the tip of the ultrasonic horn with a laser vibrometer for a 25 cycles sine wave input with a centre frequency of 73 kHz. (Bottom) Frequency spectrum of the measured displacement signal.

analytical model described above.

Figure 2 shows the input displacement profile to the granular chain measured at the tip of the ultrasonic horn and its spectrum. Due to the amplification effect of the horn, the input signal has a tapered window shape followed by a long ringing. This amplification is crucial since a single transducer cannot generate the necessary input displacement to trigger a nonlinear wave behaviour in the chain. Although the output displacement profile looks different than a 25 cycle tone burst excitation, the spectra of the output signal shows a narrowband behaviour with a -6 dB bandwidth of 3.5 kHz and a second harmonic level of -26 dB as shown in Figure 2 (bottom).

A positive push towards the hydrophone direction, as illustrated in Fig. 1 will generate a compression wave, which is a negative pressure pulse in water. Therefore, all velocity plots presented here are inverted so as to enable direct comparison with the pressure plots.

C. Pre-compression Force

The pre-compression force was estimated based on the resonance shift of the 73 kHz ultrasonic horn under mechanical stress, similar to the principle used in atomic force microscopy[27]. A pre-compression force measurement setup was created (not shown in this paper) using calibrated masses and a Bode 100 Vector Network Analyzer (Omicron Lab, Houston, TX) to detect the resonance peak. The ultrasonic horn was mechanically compressed using the calibrated masses and its impedance was measured for pre-compression forces of $0-2$ N with a step size of 0.25 N. Therefore the pre-compression force measurements have a precision of 0.25 N and a maximum error of $\pm$ 0.125 N. After acquiring the impedance

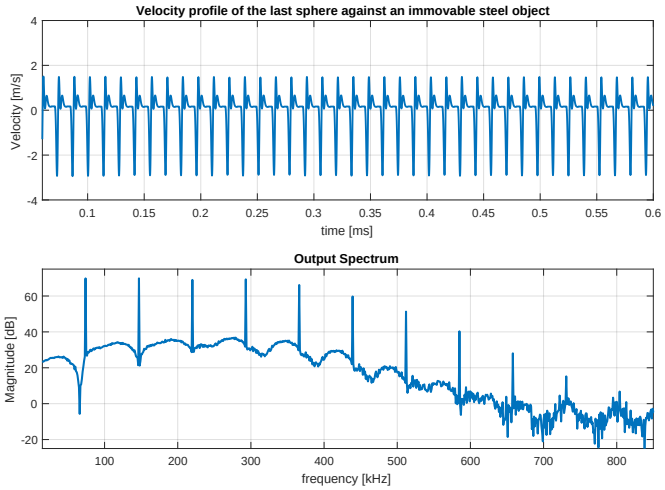

FIG. 3. (Top) Estimated velocity profile with the analytical model for a 6-sphere chain against an immovable steel wall for pre-compression force of 1.25 N. (Bottom) Corresponding frequency spectrum.

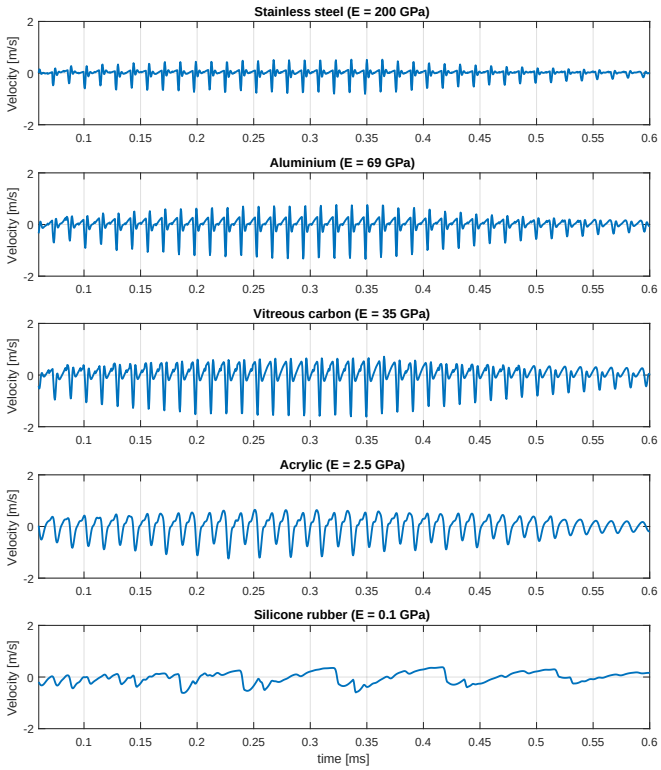

FIG. 4. Estimated velocity profile with the analytical model for a chain of six aluminium spheres terminated with different matching layers with a thickness of 0.5 mm and pre-compression force of 1.25 N.

measurements, the ultrasonic horn was placed in the experimental setup shown in the Figure 1 and the pre-compression force was adjusted with a micro-meter translation stage to maximise the acoustic pressure amplitude in water, which corresponds to maximum velocity at the surface of the matching layer.

III. RESULTS

To demonstrate the effect of the matching layer, the response of the granular chain was calculated using the analytical model described earlier[18] for continuous sine wave excitation with an input displacement amplitude of 3.3 μm, input velocity of 1.5 m/s, $F_0 = 1.25$ N, and $\lambda = 0.32$. Figure 3 shows the velocity of the last sphere for a 6-sphere granular chain terminated with an infinite steel wall. A granular chain system placed between two immovable boundaries can accommodate periodic solitary waves for a given input force and pre-compression force, which is explained as in-phase nonlinear normal modes by Jayaprakash *et al.*[28].

After developing the model, different matching materials were analysed to investigate the effect of matching layer on the nonlinear wave generation in the granular chain. A stainless steel, aluminium, vitreous carbon, acrylic, and silicon rubber matching layers were simulated with 0.5 mm thickness, where the wavelength for the slowest material corresponds to 13.8 mm. Figure 4 shows the velocity at the surface of the matching layer, which can be considered as an approximate representation of pressure waves generated in water. The results showed that soft matching layers such as rubber inhibit the generation of nonlinear periodic waves. This is intuitive, since the Young's modulus of the silicone rubber is $2-3$ orders of magnitude smaller than aluminium and the matching layer will easily bend with the applied pre-compression force. In this case, the spheres may not easily lose contact with each other, which is necessary for the generation of nonlinear periodic solitary waves as shown in Figure 3.

When a solitary wave reaches to the end of the chain, the kinetic to potential energy conversion at the wall is a function of the Young's modulus, as demonstrated by Job *et al.*[20]. The ratio between the maximum force at the wall and the force observed by the sphere is proportional to $(E_m/(E_m + E_s))^{0.4}$. This explains a large and a small reduction in the amplitude of the periodic solitary waves respectively for the rubber and acrylic matching layers with small Young's modulus values. For larger Young's modulus values, Job *et al.* predicts an increased output force which contradicts with the findings of this study. The reason for this is due to the definition of the end location. Job *et al.* calculated the force at the end of the chain, which is the boundary between the last sphere and the wall. In this study, the proposed model predicts the velocity profile at the other side of the matching layer which is in contact with water. For this case, the acoustic impedance, which is proportional to the square root of the Young's modulus and density, of the matching material becomes important. Therefore, when the be-

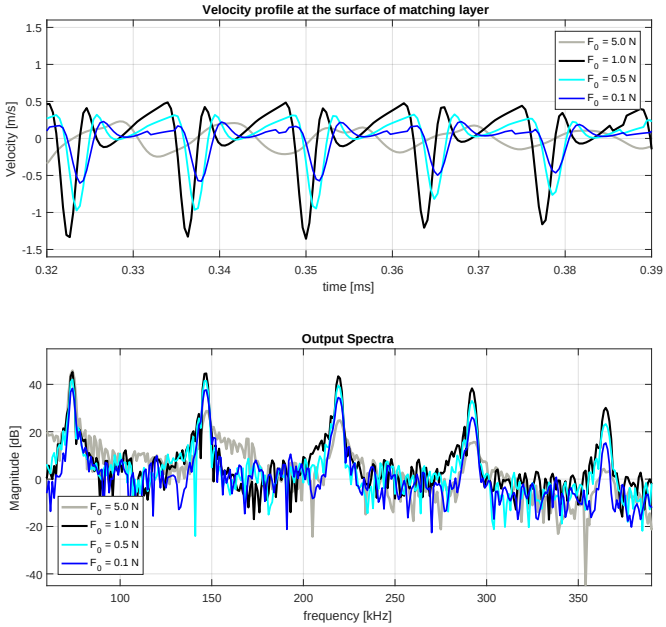

FIG. 5. (Top) Velocity profile estimated at the surface of the vitreous carbon matching layer for different pre-compression forces. (Bottom) Regarding frequency spectra.

haviour of hard matching layer materials was compared, vitreous carbon achieved the largest peak velocity due to its acoustic impedance closer to the optimal value of $\sqrt{Z_{\text{aluminium}} \cdot Z_{\text{water}}} = 5.1$ MRayl. Aluminium, steel, and vitreous carbon matching layers all support the generation of nonlinear solitary waves, which can be seen in Figure 4 as periodic nonlinear waves. However, for the aluminium and steel matching layers with larger Young's modulus, the output velocity drops due to the increasing acoustic impedance mismatch.

After deciding on using vitreous carbon as a matching layer, the effect of the pre-compression force was simulated. The velocity profile and the corresponding frequency spectra at the surface of the vitreous carbon matching layer were estimated for different pre-compression forces. This study aimed to maximise the output velocity profile or the pressure of the system for ultrasound applications, where the waveform shape and the amplitude of the generated waves are both important. Generation of a narrow negative solitary peak means a signal with high harmonic content, which is of interest for biomedical ultrasound applications. To demonstrate this, the system response for varying pre-compression force was plotted in Figure 5 (top). For increasing pre-compression force up to 1 N, the peak velocity increases and the pulse width narrows. For the pre-compression force of 5 N, the shape of the waveform changes and harmonics disappear. Figure 5 (bottom) shows the signal spectra regarding to these velocity plots, where the spectrum of the waveform with $F_0 = 1$ N has the highest magnitude at each harmonic and thus it is the desirable signal.

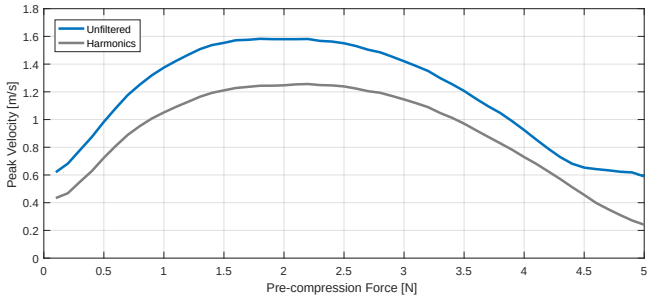

FIG. 6. Relation between the pre-compression force and maximum velocity profile at the surface of the matching layer that represent the acoustic pressure. The maximum harmonic content is calculated after filtering the fundamental signal at 73 kHz with a high-pass filter.

For this reason, the relation between the pre-compression force and velocity profile must be analysed first in order to increase the transferred ultrasound energy into biological tissue. Figure 6 shows that, there exists an optimum pre-compression force for a given setup. Since the generation of higher order harmonics increases the bandwidth of the ultrasound signal, a harmonic level was also included in the analysis as shown in Figure 6.

The maximum velocity amplitude was predicted by the analytical model to occur at a pre-compression force of 1.8 N (Figure 6). It can be seen that there is very good qualitative agreement between the predictions of the analytical model and experiment. The experimental waveform seems more uniform in response across the harmonics, perhaps indicating a degree of additional damping in the experimental system, which is difficult to quantify, but is likely to be due to damping of the horn caused by contact with the first sphere. Note that the maximum output signal was obtained using a pre-compression force of 1.25 N. It was not possible to measure the excitation signal with a vibrometer while in contact; however the loading effect will change the envelope shape of the excitation signal and also the peak displacement value, which will directly reduce with the pre-compression force for the maximum velocity since the F_{in}/F_0 is the scaling factor.

The granular chain setup was formed and model parameters were estimated based on real hydrophone measurements. The pre-compression force applied on the chain was adjusted by using a differential adjuster translation stage, as shown in Fig 1. The experimental pre-compression force was estimated as $F_0 = 1.25$ N while estimates for the damping coefficient yielded as $\lambda_m = 1.05$ and $\lambda = 0.32$ by matching the model with hydrophone measurements. These empirical parameters were used in this section for the coherency of the study.

Fig. 7 and Fig. 8 show a comparison of the predicted waveform with the model and the ultrasound pressure waves measured with a hydrophone in water. Fig. 7 (top) shows the measured and the predicted waveforms for the whole duration. The measured signal exhibits a linear

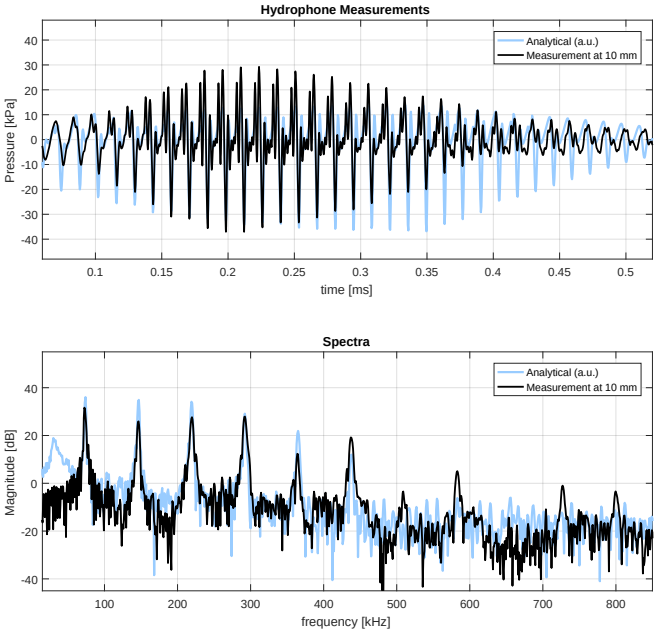

FIG. 7. (Top) Ultrasound pressure waveform measured in water and the velocity profile estimated at the surface of the vitreous carbon matching layer are plotted for comparison. (Bottom) Regarding frequency spectra.

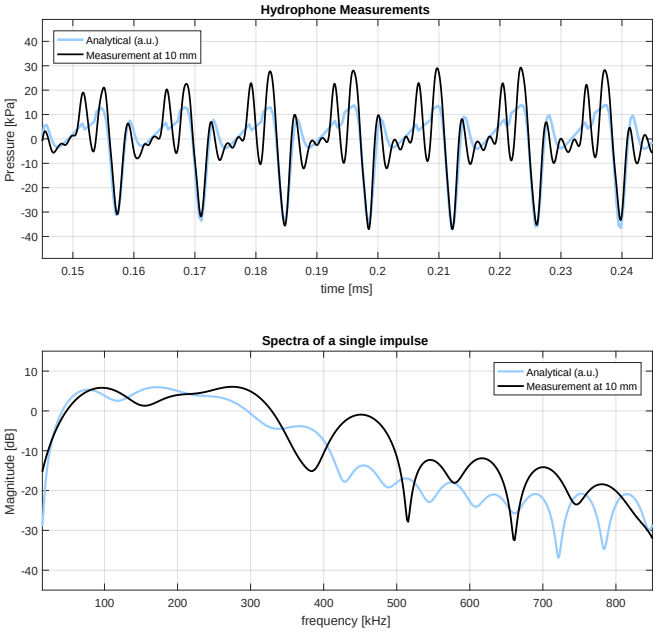

FIG. 8. (Top) Comparison of measured ultrasound wave and predicted velocity profile with the model. Fig. 7 re-plotted with different time scale for clear visualisation. (Bottom) Frequency spectra of single pulse located around 0.2 ms.

behaviour for the first $2-3$ cycles. Later on the nonlinear behaviour rises with increasing input force (Figure 2), which overlaps with the predicted waveform by the model. After $t = 0.35$ ms, the nonlinear behaviour dies out faster than the model's prediction with several cycles of ringing. Fig. 7 (bottom) shows spectra of the measured and the predicted waveforms, where a rich harmonic content up to 11-th harmonic is observed for the measured signal.

For clear visualisation of the signal envelope and individual pulse shapes, Fig. 7 was plotted again with a different time scale. To evaluate the correspondence of the predicted waveform to the measurements three metrics were used; the normalised cross-correlation (NCC), -6 dB bandwidth of individual pulses as shown in Figure 8 (bottom), and the root mean squared total harmonic distortion (THD). The NCC shows similarities between two signals in terms of shape and phase response. Although, it is good metric to evaluate fidelity between two signals, the differences between the level of the harmonics and the signal bandwidth can be overlooked by NCC. Since the generation of harmonics are of interest for this study, the THD and the -6 dB bandwidth of the signals are also used to analyse signal fidelity between the hydrophone measurements and the model predictions.

Similarities between two signals were calculated separately for all pulses between 0.11 ms and 0.38 ms in Figure 7 (top). The average similarity between the measurements and the model was calculated as $83 \pm 3\%$ by using NCC. The -6 dB bandwidth of individual pulses were measured as 280 kHz, which was predicted with the model as 252 kHz. The root mean squared THD was calculated to evaluate the harmonic energy generation up to tenth harmonic, where a THD value of 73% and 78% was measured with the hydrophone and was predicted by the model, respectively.

Although, the shape of the individual pulses match with $83 \pm 3\%$ correlation and the bandwidth with $10\% \pm 4$ error, the shape of the signal envelope was different as compared in Figure 7. As outlined earlier, this is likely to be due predominantly by the loading effect on the ultrasonic horn when in contact with spheres, which will be changing the measured displacement output of the horn shown in Fig. 2.

A comparison between the velocity profiles of the last (output) sphere and the matching layer are shown in Figure 9. The amplitude at the surface of the matching layer facing the water was reduced as expected, due to the impedance mismatch at either surface. The Figure also highlights the section of the waveform when the contact between the last sphere and the matching layer was lost.

IV. DISCUSSION

In general, a reduction in the pre-compression force will increase the non-linearities in a granular chain, resulting in a larger energy transfer into higher frequencies[18]. However, after attaching a finite matching layer to the system, generation of wideband ultrasound waves in water cannot be maximised by reducing the pre-compression force. To maximise the amplitude of the ultrasound pressure waves, an optimum pre-compression

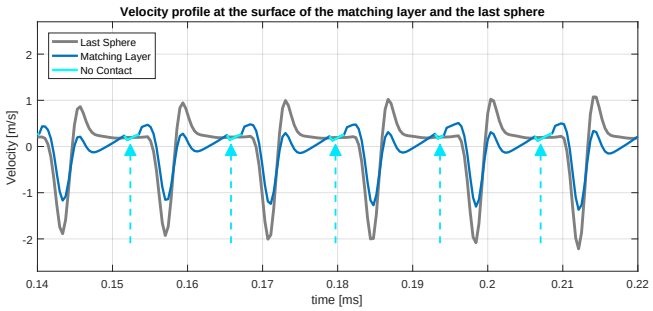

FIG. 9. Velocity profiles at the surface of the matching layer and the last sphere are plotted for comparison. Blue arrows point at the highlighted section of the waveform where the contact between the last sphere and the matching layer are lost.

force can be estimated based on the matching-layer properties or an application specific matching material can be selected. The model also shows that the selected material, its thickness, and therefore the mass of the matching layer affect the bandwidth of the output signal. A thin matching layer will be ideal for coupling of higher frequency signals; however, a thick layer will increase the nonlinear behaviour in the granular chain. Therefore, the traditional quarter wavelength matching approach is no longer suitable, since the final signal bandwidth is a function of the matching layer thickness. Although it was not performed in this study due to the lack of availability of different thickness vitreous carbon materials, the model can be used to predict an optimum matching layer thickness after incorporating the effect of attenuation and multiple reflections inside the material.

Another important difference of this study in comparison to others in the existing literature is the use of large pre-compression force ($F_0 > 1$ N), which also brings certain advantages. The compression in the chain was set three orders of magnitude larger than the gravitational compression on a vertical chain, which eliminates the effect of gravity on the output of the system at any orientation and increases the mobility of the system. Note that it has been reported that the damping of the signals in a gravitationally compressed chain is different to that expected for a horizontal chain[29]. For a large pre-compression force, the characteristic of the wave propagation in the chain does not suddenly change due to small variations in pre-compression force and increases the tolerance of the system to external factors such as thermal effects. The large pre-compression force also increases the cut-off frequency of such chains, above which solitary wave behaviour is not expected. The cut-off frequency is usually estimated by assuming harmonic excitation of an infinite chain[1]. Such a cut-off frequency for a chain of aluminium spheres can be predicted in this way as 318 kHz for $F_0 = 1.25$ N and dropping to 209 kHz for $F_0 = 0.1$. However, both in simulations and the experiment, harmonic generation can be seen at higher frequencies. This is a result of having a chain of finite length attached to an immovable (the ultrasonic horn) and a movable wall (the matching layer), where the cut-off frequency is not predictable due to the increased complexity of the system when a chain of finite length is used.

V. CONCLUSIONS

In this study, an analytical model was created to predict the motion of a finite material attached to a granular chain as a matching layer. An experimental setup was created to verify the estimated motion of the matching material with the new model. The setup consisted of a one-dimensional chain of six aluminium spheres, a vitreous carbon matching layer and a ultrasonic horn. The ultrasonic horn generated a narrowband input of 25 cycle sinusoidal tone burst with a centre frequency of 73 kHz and a -6 dB bandwidth of 3.5 kHz. The output was measured in water as a train of wideband ultrasonic pulses with a -6 dB bandwidth of 280 kHz, which is predicted with the model as 252 kHz. It is the first experimental demonstration of resonant chains operating in water with a matching layer at such a high ultrasonic frequency.

The results presented in this paper indicate that such chain-like systems may be of interest to the biomedical ultrasound community, where a train of high frequency impulses might have applications in imaging, microbubble dynamics and high intensity therapy.

The authors gratefully acknowledge funding from the Engineering and Physical Sciences Research Council (UK) via grant number EP/K029835/1.

[1] V. F. Nesterenko, J Appl Mech Tech Phys **24(5)**, 733 (1983).
[2] C. Coste, E. Falcon, and S. Fauve, Phys. Rev. E **56**, 6104 (1997).
[3] F. Santibanez, R. Munoz, A. Caussarieu, S. Job, and F. Melo, Phys. Rev. E **84**, 026604 (2011).
[4] J. Lydon, K. R. Jayaprakash, D. Ngo, Y. Starosvetsky, A. F. Vakakis, and C. Daraio, Phys. Rev. E **88**, 012206 (2013).
[5] J. Lydon, G. Theocharis, and C. Daraio, Phys. Rev. E **91**, 023208 (2015).
[6] X. Zhang and Z. Liu, Nature Materials **7**, 435 (2008).
[7] N. Boechler, G. Theocharis, and C. Daraio, Nature Materials **10**, 665 (2011).
[8] K. Li, P. Rizzo, and X. Ni, J. Appl. Mech. **81**, 071011 (2014).
[9] A. Spadoni and C. Daraio, Proceedings of the National Academy of Sciences **107**, 7230 (2010).
[10] J. Yang, D. Khatri, P. Anzel, and C. Daraio, Int J Solids Struct **49**, 1463 (2012).
[11] F. Tranquart, N. Grenier, V. Eder, and L. Pourcelot, Ultrasound in Medicine & Biology **25**, 889 (1999).
[12] Q. Ma, Y. Ma, X. Gong, and D. Zhang, Ultrasound in Medicine & Biology **31**, 889 (2005).
[13] A. Bouakaz and N. de Jong, IEEE Trans. Ultrason., Ferroelect., Freq. Control. **50**, 496 (2003).
[14] S. Harput, J. McLaughlan, D. M. J. Cowell, and S. Freear, IEEE Trans. Ultrason., Ferroelect., Freq. Control. **61**, 1802 (2014).
[15] K.-W. Lin, T. Hall, R. McGough, Z. Xu, and C. Cain, IEEE Trans. Ultrason., Ferroelect., Freq. Control. **61**, 1123 (2014).
[16] L. Cai, J. Yang, P. Rizzo, X. Ni, and C. Daraio, Granular Matter **15**, 357 (2013).
[17] C. M. Donahue, P. W. J. Anzel, L. Bonanomi, T. A. Keller, and C. Daraio, Applied Physics Letters **104**, 014103 (2014).

[18]D. A. Hutchins, J. Yang, O. Akanji, P. J. Thomas, L. A. J. Davis, S. Freear, S. Harput, N. Saffari, and P. Gelat, EPL (Europhysics Letters) **109**, 54002 (2015).
[19]M. A. Porter, P. G. Kevrekidis, and C. Daraio, Physics Today **68**, 44 (2015).
[20]S. Job, F. Melo, A. Sokolow, and S. Sen, Phys. Rev. Lett. **94**, 178002 (2005).
[21]D. Hutchins, J. Yang, O. Akanji, L. Davis, P. Thomas, S. Freear, S. Harput, N. Saffari, and P. Gelat, in *IEEE Int. Ultrasonics Symposium (IUS)* (2014) pp. 2607–2610.
[22]D. A. Hutchins, J. Yang, O. Akanji, P. J. Thomas, L. A. J. Davis, S. Freear, S. Harput, N. Saffari, and P. Gelat, Ultrasonics **69**, 215 (2016).
[23]O. Akanji, J. Yang, D. A. Hutchins, P. J. Thomas, L. A. J. Davis, S. Harput, S. Freear, P. Gelat, and N. Saffari, IEEE Trans. Ultrason., Ferroelect., Freq. Control. **63**, 1957 (2016).
[24]S. Harput, J. McLaughlan, S. Freear, P. Gelat, N. Saffari, J. Yang, O. Akanji, P. J. Thomas, and D. A. Hutchins, in *IEEE Int. Ultrasonics Symposium (IUS)* (2015).
[25]S. Harput, S. Freear, P. Gelat, N. Saffari, J. Yang, O. Akanji, P. J. Thomas, and D. A. Hutchins, in *IEEE Int. Ultrasonics Symposium (IUS)* (2016).
[26]J. Yang, D. A. Hutchins, O. Akanji, P. J. Thomas, L. A. J. Davis, S. Harput, P. Gelat, S. Freear, and N. Saffari, Phys. Rev. E **93**, 063002 (2016).
[27]U. Rabe, K. Janser, and W. Arnold, Review of Scientific Instruments **67**, 3281 (1996).
[28]K. Jayaprakash, Y. Starosvetsky, A. Vakakis, M. Peeters, and G. Kerschen, Nonlinear Dynamics **63**, 359 (2011).
[29]J. Hong, H. Kim, and J.-P. Hwang, Phys. Rev. E **61**, 964 (2000).